

Systematic study of hadrons and their quark-component nuclear modification factors

An-Ke Lei,¹ Dai-Mei Zhou,^{1,*} Yu-Liang Yan,^{2,†} Du-Juan Wang,³
Xiao-Mei Li,² Gang Chen,⁴ Xu Cai,¹ and Ben-Hao Sa^{1,2,‡}

¹*Key Laboratory of Quark and Lepton Physics (MOE) and Institute of Particle Physics,
Central China Normal University, Wuhan 430079, China*

²*China Institute of Atomic Energy, P. O. Box 275 (10), Beijing 102413, China*

³*Department of Physics, Wuhan University of Technology, Wuhan 430070, China*

⁴*Physics Department, China University of Geoscience, Wuhan 430074, China*

(Dated: May 29, 2023)

We have systematically studied the connection (correspondence) between hadron and its quark component nuclear modification factors and the flavor (mass) ordering at both parton and hadron levels in the nucleus-nucleus collisions at the LHC energies by the PACIAE model. It turns out that the correspondence and the mass ordering are generally held, irrespective of the rapidity, centrality, reaction energy, and the collision system size. The nuclear modification factors of hadrons in the final hadronic state show clear mass ordering, which should be studied further both theoretically and experimentally.

I. INTRODUCTION

The hot and dense Quark-Gluon Plasma (QGP), a phase of deconfined nuclear matter, has been found to be created in ultra-relativistic heavy-ion collisions at both the Relativistic Heavy Ion Collider (RHIC) [1–4] and the Large Hadron Collider (LHC) [5–9]. One of the most important signatures for QGP formation is the suppression of hadron production at high transverse momentum (p_T) due to the energy loss effect (jet quenching) [10, 11]. To quantify such a suppression effect, the nuclear modification factor measurement was proposed [12]. It is defined as the ratio of the p_T -differential multiplicity dN/dp_T in nucleus-nucleus collisions (AA) to the one in nucleon-nucleon collisions (pp), scaled by the binary collision number $\langle N_{coll} \rangle$ for a given range of centrality interval [12, 13]

$$R_{AA}^X(p_T) = \frac{1}{\langle N_{coll} \rangle} \frac{dN_X^{AA}/dp_T}{dN_X^{pp}/dp_T}, \quad (1)$$

where X stands for a specific particle, $\langle N_{coll} \rangle$ can be obtained from the optical Glauber model and/or the Monte-Carlo Glauber model [14–19]. The value of R_{AA} would be unity if an AA collision is just a simple superposition of the pp collisions. Conversely, one could expect a non-unity R_{AA} in the presence of the cold and hot nuclear medium effects. Therefore, R_{AA} could serve as an excellent observable for exploring the jet quenching effect.

The QGP medium induced jet quenching effect is expected to suppress the R_{AA} of partons in the final partonic state (FPS). On the other hand, the R_{AA} of hadrons in the final hadronic state (FHS), the one actually measurable in experiments, receives convoluted contributions

from the partonic jet quenching effect and the hadronic energy loss effect in the hadronization and hadronic rescattering stage. Naturally, one would seek the connection (correspondence) between the R_{AA} of partons in FPS and the R_{AA} of hadrons in FHS. Taking R_{AA} of Λ as an example, the connection between R_{AA} of Λ and that of its quark component could be considered in simple forms like follow:

1. connect R_{AA}^Λ to single R_{AA}^u (R_{AA}^d , R_{AA}^s);
2. connect R_{AA}^Λ to R_{AA}^{u+d} (R_{AA}^{u+s} , R_{AA}^{d+s}), calculated by the sum of u - and d - (u - and s -, d - and s -) quark p_T -distributions without weight factor;
3. connect R_{AA}^Λ to R_{AA}^{u+d+s} , calculated by the sum of u -, d -, and s -quark p_T -distributions without weight factor.

However, all of them are incomplete:

1. the d - and s - (u - and s -, u - and d -) constituent quarks are ignored;
2. the s - (d -, u -) constituent quark is excluded;
3. the contribution of sea quark s is underestimated.

As far as we know, a correct connection (correspondence) is unable to be introduced from the first principle theory, even from the recombination (coalescence) model [20–25], because of the complication in dealing with the flavor composition of constituent quarks. Recently, a connection (correspondence) between the hadron R_{AA} (in FHS) and its quark component one (in FPS) has been proposed by us for the first time [26], and the R_{AA} mass ordering at hadron level, initiating from the dead-cone effect [27], is also explored [26]. In this work, we extend the study to the rapidity, centrality, reaction energy, and the collision system size dependences of above two physical phenomena.

The paper is organized as follows. In Sec. II the methodology to study the R_{AA} correspondence of the

* zhoum@mail.ccnu.edu.cn

† yanyl@ciae.ac.cn

‡ sabh@ciae.ac.cn

hadron and its quark component is provided, after the introduction section Sec. I. In Sec. III, the results of correspondence and R_{AA} mass ordering dependent on the rapidity, centrality, reaction energy and the collision system size are presented. We summarize in Sec. IV.

II. METHODOLOGY

In this work, we follow the formalism of the correspondence between the hadron R_{AA}^h in FHS and its quark component R_{AA}^{h-q} (the script $h-q$ refers to the quark component of the hadron h) in FPS established in Ref. [26]. The brief physical deduction is described as follows:

Considering the hadron normalized p_T -differential distribution

$$\frac{1}{N_h} dN_h/dp_T,$$

its corresponding quark component normalized p_T -differential distribution is

$$\frac{1}{N_{h-q}} \sum_q \frac{1}{N_q} dN_q/dp_T.$$

In the above expressions, N_h (N_q) refers to the multiplicity of the hadron h (quark q). N_{h-q} denotes the number of constituent quarks in a hadron h and the sum is taken over all constituent quarks.

Multiplying above two expressions by N_h , one can get the hadron un-normalized p_T -differential distribution

$$dN_h/dp_T$$

and the corresponding quark component un-normalized p_T -differential distribution

$$\frac{1}{N_{h-q}} \sum_q \frac{N_h}{N_q} dN_q/dp_T.$$

Substituting above two un-normalized p_T -differential distributions into equation (1), respectively, one obtains the hadron nuclear modification factor

$$R_{AA}^h(p_T) = \frac{1}{\langle N_{coll} \rangle} \frac{dN_h^{AA}/dp_T}{dN_h^{pp}/dp_T}, \quad (2)$$

and its corresponding quark component nuclear modification factor

$$R_{AA}^{h-q}(p_T) = \frac{1}{\langle N_{coll} \rangle} \frac{\sum_q w_q^{AA} dN_q^{AA}/dp_T}{\sum_q w_q^{pp} dN_q^{pp}/dp_T}, \quad (3)$$

where $w_q = N_h/N_q$ is the weight factor.

To investigate the correspondence between hadron and its quark component and the mass ordering at hadron level in R_{AA} , a numerical Monte-Carlo event generator, PACIAE [28], is employed to simulate the pp and AA

collisions. PACIAE is a microscopic parton and hadron cascade model based on the PYTHIA6.4 event generator [29].

For nucleon-nucleon (NN) collisions, with respect to PYTHIA, the partonic and hadronic rescatterings are introduced before and after the hadronization, respectively. The final hadronic state is developed from the initial partonic hard scattering and parton showers, followed by parton rescattering, string fragmentation, and hadron rescattering stages. Thus, the PACIAE model provides a multi-stage transport description on the evolution of the NN collision system.

For AA collisions, the initial positions of nucleons in the colliding nuclei are sampled according to the Woods-Saxon distribution. Together with the initial momentum setup of $p_x = p_y = 0$ and $p_z = p_{beam}$ for each nucleon, a list containing the initial state of all nucleons in a given AA collision is constructed.

A collision happened between two nucleons from different nuclei if their relative transverse distance is less than or equal to the minimum approaching distance: $D \leq \sqrt{\sigma_{NN}^{tot}/\pi}$. The collision time is calculated with the assumption of straight-line trajectories. All such nucleon pairs compose an NN collision time list.

The earliest NN collision in the list will be executed by PYTHIA (PYEVNW subroutine) with the hadronization temporarily turned-off, as well as the strings and diquarks broken-up. The nucleon list and NN collision time list are then updated accordingly for the iteration of the next NN collision. By repeating the aforementioned steps till the NN collision list is empty, the initial partonic state is constructed for an AA collision.

Then, the partonic rescatterings are performed, where the LO-pQCD parton-parton cross section [30, 31] is employed. After partonic rescattering, the string is recovered and then hadronized with the Lund string fragmentation scheme.

The Lund string fragmentation is a phenomenological hadronization model. Here the key assumption is the iterative string breaking procedure: Supposing an iterative string breaking process starting from the q_0 end of a $q_0\bar{q}_0$ string, if the string potential energy is large enough, a new $q_1\bar{q}_1$ pair may be excited from the vacuum, such that a meson M_1 of $q_0\bar{q}_1$ is formed and the q_1 quark left behind. Later on, the q_1 in its turn may excite a $q_2\bar{q}_2$ pair from the vacuum and combine into another meson M_2 with the \bar{q}_2 . This breaking process repeats and repeats until the potential energy is not large enough. The similar is for the baryon-antibaryon (BB) production in the popcorn model. But instead of starting from one end of $q_0\bar{q}_0$ string, in popcorn model the process is performed on the entire $q_0\bar{q}_0$ string. Suppose $q_0\bar{q}_0$ is a red-antired ($r\bar{r}$) string and has enough potential energy to excite three pairs of green-antigreen ($g\bar{g}$), blue-antiblue ($b\bar{b}$), and antiblue-blue ($\bar{b}b$) iteratively from the vacuum in between the $r\bar{r}$ string. Then a red-green-blue and antiblue-antigreen-antired baryon-antibaryon ($B\bar{B}$) pair may form together with a antiblue-blue meson (M)

in between the original $r\bar{r}$ pair, resulting in a $(B\bar{M}\bar{B})$ configuration [29, 32].

Taking the meson production as an example, once the q_{i-1} and \bar{q}_i flavors are sampled, a selection should be made between the possible multiplets. The different multiplets have different relative composition probabilities, which are not given by first principle but depend on the fragmentation processes, cf. Refs. [29, 32] for the details.

Finally, the above formed intermediate hadronic state proceeds into the hadronic rescattering stage and produces the final hadronic state observed in the experiments.

Thus PACIAE Monte-Carlo simulation provides a complete description of the NN and/or AA collisions, which includes the partonic initialization stage, partonic rescattering stage, hadronization stage, and the hadronic rescattering stage. Meanwhile, the PACIAE model simulation could be requested to stop at any of the above stages conveniently. In this work, the simulations are stopped at the final partonic state (FPS) after partonic rescattering or at final hadronic state (FHS) after hadronic rescattering for the calculations of R_{AA}^{h-q} and R_{AA}^h , respectively. More details could be found in the Ref. [28].

In order to be self-consistent, the tuning parameters are kept the same as those in Ref. [26]: A factor multiplying on the hard scattering cross-section $K=2.7$ (0.7), the Lund string fragmentation parameters of $\alpha=1.3$ (0.1) and $\beta=0.09$ (0.58), as well as the Gaussian width of the primary hadron transverse momentum distribution $\omega=0.575$ (0.36) are implemented in AA (pp) simulations.

III. RESULTS AND DISCUSSIONS

In Ref. [26], we have proposed a method connecting the hadron nuclear modification factor R_{AA}^h in FHS to its quark component nuclear modification factor R_{AA}^{h-q} in FPS, and explored the mass ordering in nuclear modification factor at both parton and hadron levels in the 0-5% most central Pb+Pb collisions at $\sqrt{S_{NN}}=2.76$ TeV. In this section, we will expand our research discussing the dependences of R_{AA} correspondence and R_{AA} mass ordering on rapidity, centrality, reaction energy, and the collision system size. Our simulations are all performed in full η phase space, except the in Sec. III A.

A. Rapidity dependence

Fig. 1 shows the meson R_{AA} in FHS (black solid circles) and its quark component R_{AA} in FPS (red open circles) within different η ranges in the 0-5% most central Pb+Pb collisions at $\sqrt{S_{NN}}=2.76$ TeV. From top to bottom rows are R_{AA} of $\pi^+(u\bar{d})$, $K^+(u\bar{s})$ and $\phi^0(s\bar{s})$, while from left to right columns are those in $|\eta| < 0.8$,

2.5 and full η phase space, respectively¹. Fig. 2 shows the same content, just for the baryon sector. A peak appears at p_T around $1 \sim 2$ GeV/c, which is the so-called Cronin effect [33] attributed to the multiple scattering of initial partons [34].

In Fig. 1 and 2, one can see that the correspondence between hadron R_{AA} and its quark component R_{AA} exists in all three rapidity ranges. The meson and baryon R_{AA} are smaller than their quark component R_{AA} in the p_T region above $p_T \approx 2$ GeV/c, even in the midrapidity interval of $|\eta| < 0.8$. This is due to the additional energy loss experienced by the final state hadrons in the hadronization and hadronic rescattering stages, while their quark components only experience partonic energy losses. Moreover, this discrepancy becomes more pronounced as the η range increases. This is because the energy loss increases with the increasing number of colliding and radiating particles involved in a wider η range.

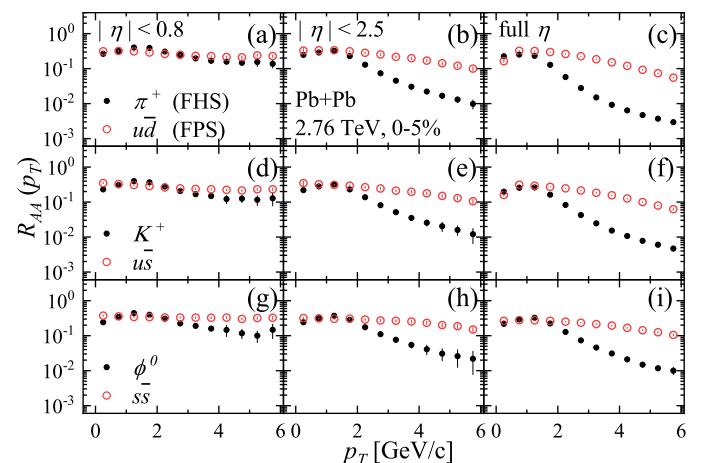


FIG. 1. The simulated correspondence between R_{AA} of mesons (in FHS, black solid circles) and their quark component (in FPS, red open circles) in the 0-5% most central Pb+Pb collisions at $\sqrt{S_{NN}}=2.76$ TeV within three pseudo-rapidity ranges.

In Fig. 3, we compare the mass ordering of the quarks (in FPS), mesons (in FHS), and the baryons (in FHS) nuclear modification factors among three different η phase spaces, as displayed from left to right column, respectively. The mass ordering seems to be generally held for quarks and mesons. However, for baryons, the mass ordering is only recognized in full η phase space. This can be explained by the relative mass discrepancy among the selected particle species. The relative mass difference among baryons ($m_p \approx 0.938$ GeV, $m_{\Lambda^0} \approx 1.116$ GeV and $m_{\Xi^-} \approx 1.322$ GeV [35]) is smaller than that among the mesons ($m_{\pi^+} \approx 140$ MeV, $m_{K^+} \approx 494$ MeV and $m_{\phi^0} \approx 1.02$ GeV) and much smaller

¹ Such a graph arrangement manner would also be utilized hereafter, just for different particle sectors and conditions applied.

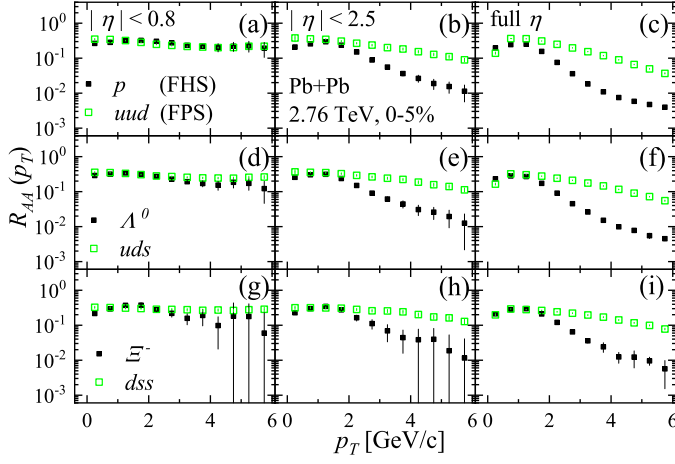


FIG. 2. The simulated correspondence between R_{AA} of baryons (in FHS, black solid squares) and their quark component (in FPS, green open squares) in the 0-5% most central Pb+Pb collisions at $\sqrt{S_{NN}}=2.76$ TeV within three pseudo-rapidity ranges.

than that among the quarks ($m_u \approx 2.2$ MeV, $m_s \approx 93$ MeV and $m_c \approx 1.27$ GeV). For quark sector, a nearly flat R_{AA} of the heavy c -quark is observed. This could be understood from the fact that the c -quark is produced in initial hard processes and transparent in the partonic and hadronic rescatterings. Hence the p_T distribution of c -quark in Pb+Pb collisions is approximately parallel to that in p+p collisions at the same energy.

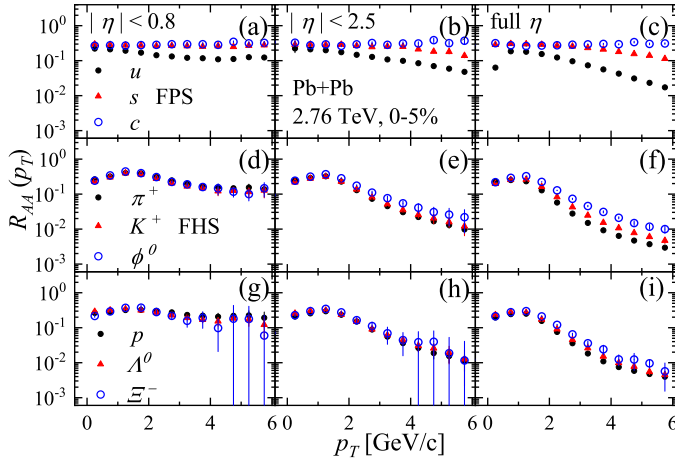


FIG. 3. The simulated R_{AA} of quarks (in FPS), mesons (in FHS) and baryons (in FHS) in the 0-5% most central Pb+Pb collisions at $\sqrt{S_{NN}}=2.76$ TeV within three pseudo-rapidity ranges.

B. Centrality dependence

In Figs 4 and 5, we show the simulated correspondence between hadron (meson and baryon in FHS) and

its quark component (in FPS) in R_{AA} in the 0-5%, 5-20% and 20-60% centrality classes Pb+Pb collisions at $\sqrt{S_{NN}}=2.76$ TeV. Still, the more stronger suppression of the hadron R_{AA} than its quark component R_{AA} can be found in all three centrality classes. One can see approximately a more depressed magnitude of both R_{AA} in more central centrality class stemming from a stronger hot medium effect. Nevertheless, the discrepancy between hadron R_{AA} and its quark component R_{AA} brought about by centrality classes is not so significant.

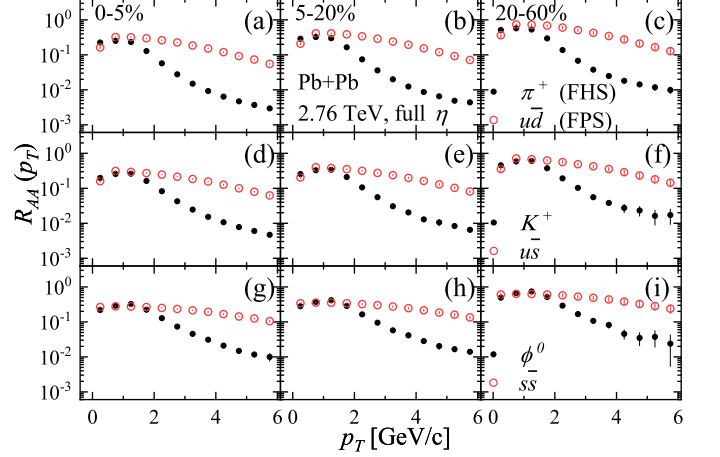


FIG. 4. The simulated correspondence between R_{AA} of mesons (in FHS, black solid circles) and their quark component (in FPS, red open circles) in the different centrality classes of Pb+Pb collisions at $\sqrt{S_{NN}}=2.76$ TeV.

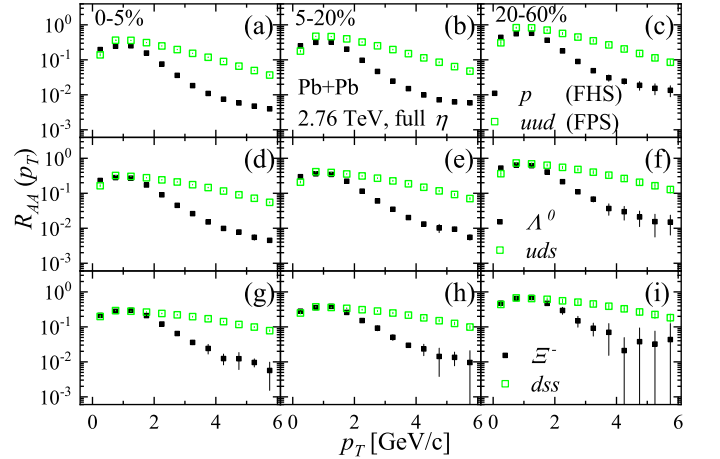


FIG. 5. The simulated correspondence between R_{AA} of baryons (in FHS, black solid squares) and their quark component (in FPS, green open squares) in the different centrality classes of Pb+Pb collisions at $\sqrt{S_{NN}}=2.76$ TeV.

Meanwhile, in Fig. 6 we give the simulated R_{AA} of quarks (in FPS), mesons (in FHS) and baryons (in FHS) in 0-5%, 5-20%, and 20-60% centrality classes Pb+Pb collisions at $\sqrt{S_{NN}}=2.76$ TeV. The good mass ordering

in the region of $p_T > 2$ GeV/c is generally held and almost insensitive to the event centrality.

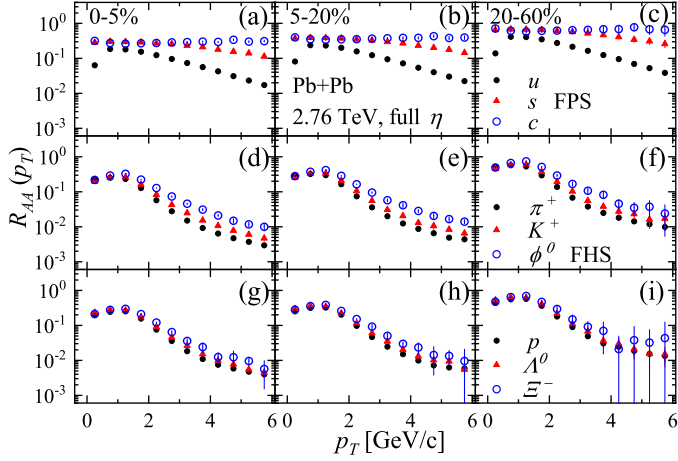


FIG. 6. The simulated R_{AA} of quarks (in FPS), mesons (in FHS), and baryons (in FHS) in the different centrality classes of Pb+Pb collisions at $\sqrt{S_{NN}}=2.76$ TeV.

C. Energy dependence

We now study the energy dependence of the correspondence between hadron R_{AA} and its quark component one, and the mass ordering at both the parton and hadron levels. In Figs. 7 and 8, we give the R_{AA} of both the hadrons (in FHS) and their quark component (in FPS) in 0-5% most central Pb+Pb collisions at $\sqrt{S_{NN}}=0.9, 2.76$ and 5.02 TeV. The correspondence is well kept at all three reaction energies. However, the discrepancy of R_{AA} between hadron and its quark component is not varying strongly with the collision energies.

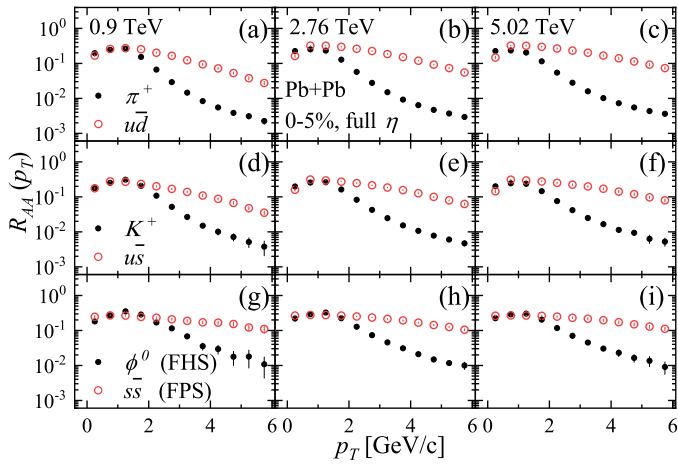


FIG. 7. The simulated correspondence between R_{AA} of mesons (in FHS, black solid circles) and their quark component (in FPS, red open circles) in the 0-5% most central Pb+Pb collisions at different reaction energies.

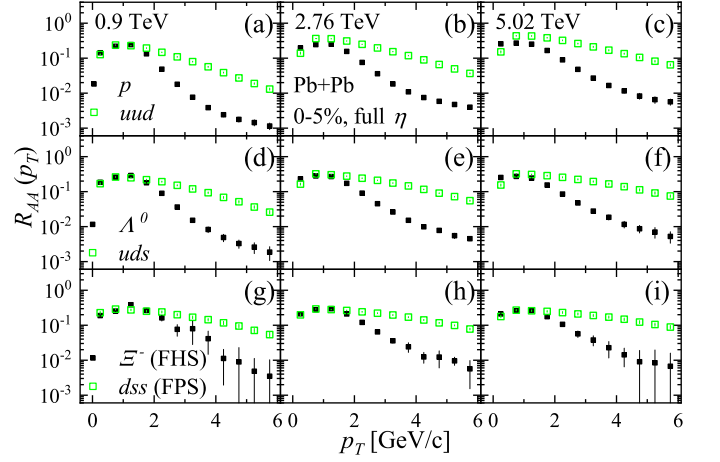


FIG. 8. The simulated correspondence between R_{AA} of baryons (in FHS, black solid squares) and their quark component (in FPS, green open squares) in the 0-5% most central Pb+Pb collisions at different reaction energies.

In Fig. 9 the mass ordering at both the parton and hadron levels are given. Here we can see the mass ordering at hadron level appears in all three reaction energies, like the one at parton level. However, it also seems that the mass ordering at both parton and hadron levels is more pronounced at the lower energy than the higher one. It should be studied further.

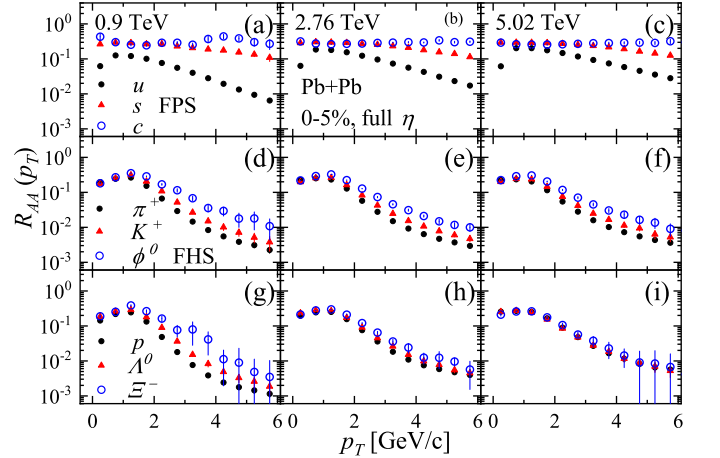


FIG. 9. The simulated R_{AA} of quarks (in FPS), mesons (in FHS), and baryons (in FHS) in the 0-5% most central Pb+Pb collisions at different reaction energies.

D. System size dependence

In Figs. 10 (meson) and 11 (baryon), we give the simulated hadron R_{AA} and its quark component R_{AA} in 0-5% most central Cu+Cu, Xe+Xe and Pb+Pb collisions at $\sqrt{S_{NN}}=2.76$ TeV. We present the mass ordering at both the parton and hadron levels in Fig. 12 for the same reaction systems above. These figures show again that, the

correspondence between hadron and its quark component in R_{AA} as well as the R_{AA} mass ordering are well kept.

As the amount of interacting matter increases with the system size, the particle propagating length is longer in larger collision system. Hence the larger the system size, the more energy losses there are [36]. Consequently, the suppression of R_{AA} would decrease with the collision system size, as shown in Figs. 10, 11 and 12 from left to right.

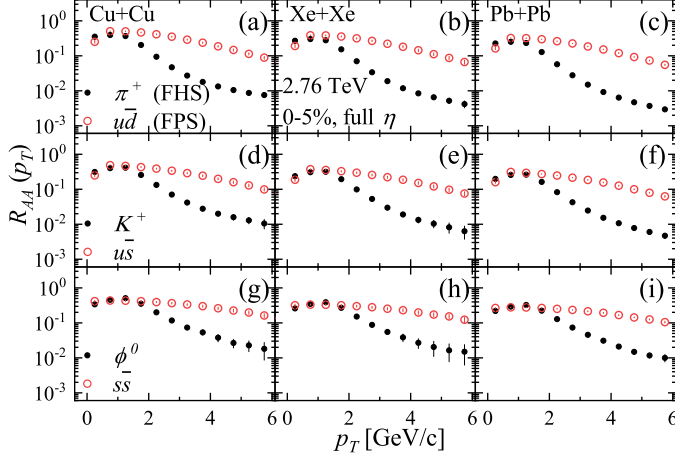


FIG. 10. The simulated correspondence between R_{AA} of mesons (in FHS, black solid circles) and their quark component (in FPS, red open circles) in the 0-5% most central Cu+Cu, Xe+Xe and Pb+Pb collisions at $\sqrt{S_{NN}}=2.76$ TeV.

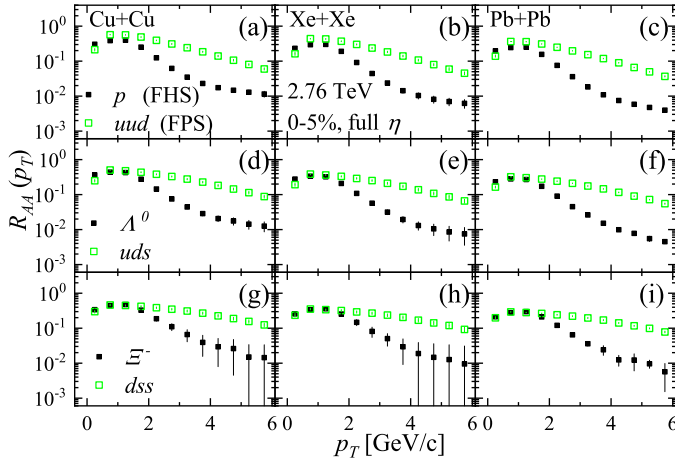


FIG. 11. The simulated correspondence between R_{AA} of baryons (in FHS, black solid squares) and their quark component (in FPS, green open squares) in the 0-5% most central Cu+Cu, Xe+Xe and Pb+Pb collisions at $\sqrt{S_{NN}}=2.76$ TeV.

IV. SUMMARY

In summary, via the parton and hadron cascade model PACIAE, we study the connection (correspondence) be-

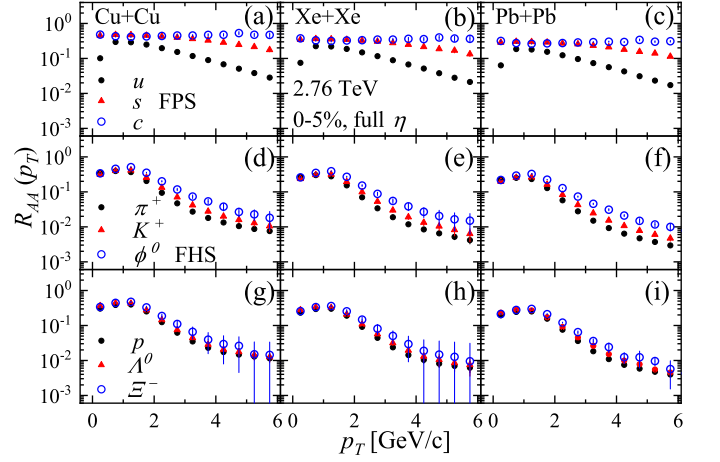


FIG. 12. The simulated R_{AA} of quarks (in FPS), mesons (in FHS), and baryons (in FHS) in the 0-5% most central Cu+Cu, Xe+Xe and Pb+Pb collisions at $\sqrt{S_{NN}}=2.76$ TeV.

tween hadron nuclear modification factor and its quark component one, as well as the flavor (mass) ordering at both parton and hadron levels. Meanwhile, how the above two physical phenomena change with the (pseudo-)rapidity, centrality, reaction energy and the collision system size are investigated systematically.

Generally speaking, the correspondence between hadron and its quark component and the mass ordering at both the parton and hadron level in nuclear modification factors are held, irrespective of the rapidity, centrality, reaction energy, and the collision system size.

For the correspondence, the R_{AA} of the hadron is always less than that of its quark component in the p_T region above 2 GeV/c. The discrepancy between them becomes more pronounced in a wider η range. However, this behavior do not noticeably show in the different centrality, reaction energy and the system size studies. The mass ordering is easier to distinguish in the wider η and the lower reaction energy, while it does not exhibit the clear dependences on the centrality and the collision system size.

We note that, the figures displaying the correspondence between hadron and its quark component in R_{AA} , show a similar phenomenon: The discrepancy between hadron R_{AA} and its quark component R_{AA} in low p_T region is less than the one in middle and/or high p_T region. It is not understood very well yet and has to leave it to the next study.

The nuclear modification factors at hadron level show very well mass ordering, like the one at parton level. Its clear observation is relevant to the relative mass discrepancy among the selected candidates. Larger relative mass discrepancy among the candidates leads to more significant mass ordering.

Of course, the correspondence between hadron and its quark component and the hadronic mass ordering in the nuclear modification factor should be studied further,

both theoretically and experimentally. In the next work, we would consider the open-charm and/or the open-bottom heavy-hadron [37] as the candidates.

ACKNOWLEDGMENTS

We thank Dr. Chun-Bin Yang for discussions. This work was supported by the National Natural Science Foundation of China (11775094, 11905188, 11775313, 11905163), the Continuous Basic Scientific Research Project (No.WDJC-2019-16), National Key Research and Development Project (2018YFE0104800) and by the 111 project of the foreign expert bureau of China.

-
- [1] K. Adcox *et al.* (PHENIX), Nucl. Phys. A **757**, 184 (2005).
 - [2] I. Arsene *et al.* (BRAHMS), Nucl. Phys. A **757**, 1 (2005).
 - [3] B. B. Back *et al.* (PHOBOS), Nucl. Phys. A **757**, 28 (2005).
 - [4] J. Adams *et al.* (STAR), Nucl. Phys. A **757**, 102 (2005).
 - [5] K. Aamodt *et al.* (ALICE), Phys. Rev. Lett. **105**, 252302 (2010).
 - [6] G. Aad *et al.* (ATLAS), Phys. Rev. Lett. **105**, 252303 (2010).
 - [7] K. Aamodt *et al.* (ALICE), Phys. Lett. B **696**, 30 (2011).
 - [8] S. Chatrchyan *et al.* (CMS), Phys. Rev. C **84**, 024906 (2011).
 - [9] B. Abelev *et al.* (ALICE), Phys. Rev. Lett. **109**, 072301 (2012).
 - [10] J. D. Bjorken, Tech. Rep. FERMILAB-PUB-82-059-T (FERMILAB, 1982).
 - [11] M. Gyulassy and M. Plumer, Phys. Lett. B **243**, 432 (1990).
 - [12] X.-N. Wang, Phys. Rev. C **58**, 2321 (1998).
 - [13] C. Klein-Bösing (ALICE), PoS **LHCP2018**, 222 (2018).
 - [14] R. J. Glauber and G. Matthiae, Nucl. Phys. B **21**, 135 (1970).
 - [15] M. L. Miller, K. Reygers, S. J. Sanders, and P. Steinberg, Ann. Rev. Nucl. Part. Sci. **57**, 205 (2007).
 - [16] B. I. Abelev *et al.* (STAR), Phys. Rev. C **79**, 034909 (2009).
 - [17] B. Abelev *et al.* (ALICE), Phys. Rev. C **88**, 044909 (2013).
 - [18] C. Loizides, J. Nagle, and P. Steinberg, SoftwareX **1-2**, 13 (2015).
 - [19] C. Loizides, J. Kamin, and D. d'Enterria, Phys. Rev. C **97**, 054910 (2018), [Erratum: Phys.Rev.C **99**, 019901 (2019)].
 - [20] R. C. Hwa and C. B. Yang, Phys. Rev. C **67**, 034902 (2003).
 - [21] V. Greco, C. M. Ko, and P. Levai, Phys. Rev. Lett. **90**, 202302 (2003).
 - [22] V. Greco, C. M. Ko, and P. Levai, Phys. Rev. C **68**, 034904 (2003).
 - [23] R. J. Fries, B. Muller, C. Nonaka, and S. A. Bass, Phys. Rev. Lett. **90**, 202303 (2003).
 - [24] R. J. Fries, B. Muller, C. Nonaka, and S. A. Bass, Phys. Rev. C **68**, 044902 (2003).
 - [25] F.-l. Shao, Q.-b. Xie, and Q. Wang, Phys. Rev. C **71**, 044903 (2005).
 - [26] B.-H. Sa, D.-M. Zhou, Y.-L. Yan, W.-D. Liu, S.-Y. Hu, X.-M. Li, L. Zheng, G. Chen, and X. Cai, J. Phys. G **49**, 065104 (2022).
 - [27] Y. L. Dokshitzer, V. A. Khoze, and S. I. Troian, J. Phys. G **17**, 1602 (1991).
 - [28] B.-H. Sa, D.-M. Zhou, Y.-L. Yan, X.-M. Li, S.-Q. Feng, B.-G. Dong, and X. Cai, Comput. Phys. Commun. **183**, 333 (2012).
 - [29] T. Sjostrand, S. Mrenna, and P. Z. Skands, JHEP **05**, 026.
 - [30] B. L. Combridge, J. Kripfganz, and J. Ranft, Phys. Lett. B **70**, 234 (1977).
 - [31] R. D. Field, *Applications Of Perturbative QCD* (Addison-Wesley Publishing Company, Inc., 1989).
 - [32] C. Bierlich *et al.*, SciPost Phys. Codebases **08** (2022).
 - [33] J. W. Cronin, H. J. Frisch, M. J. Shochet, J. P. Boymond, R. Mermod, P. A. Piroue, and R. L. Sumner (E100), Phys. Rev. D **11**, 3105 (1975).
 - [34] X.-N. Wang, Phys. Rev. C **61**, 064910 (2000).
 - [35] P. A. Zyla *et al.* (Particle Data Group), PTEP **2020**, 083C01 (2020).
 - [36] X.-N. Wang, Nucl. Phys. A **750**, 98 (2005).
 - [37] A. Andronic *et al.*, Eur. Phys. J. C **76**, 107 (2016).